

Temporal and Spatial Growth of Wind Waves

M. STIASSNIE AND Y. AGNON

Faculty of Civil and Environmental Engineering, Technion—Israel Institute of Technology, Haifa, Israel

P. A. E. M. JANSSEN

European Centre for Medium-Range Weather Forecasts, Reading, United Kingdom

(Manuscript received 12 September 2005, in final form 2 May 2006)

ABSTRACT

A solution of Rayleigh's instability equation, which circumvents the apparent critical-layer singularity, is provided. The temporal and spatial growth rates of water waves exposed to a logarithmic wind profile are calculated and discussed. The findings are similar to previously published results, except for shear velocity-to-wave celerity ratios larger than 2, where the newly calculated growth rates start to decrease after having reached a distinct maximum. The ratio of the spatial to temporal growth rates is examined. It is shown to deviate by up to 20% from the leading-order value of 2. The implications of the growth rate to the modal distributions of energy input from wind to waves, for young and mature seas, and in temporal/spatial growth scenarios, are analyzed.

1. Introduction

The study of the growth of ocean surface waves by the wind blowing over them is often treated as a linear stability problem. Miles (1957) was the first to use Rayleigh's (1880) equation for this problem. When studying linear stability problems, it seems helpful to consider two typical scenarios: one of temporal growth and the other of spatial growth. The shear velocity¹ of the wind U^* and the amplitude of the wave a for both scenarios are given by

(i) the temporal growth scenario

$$U^*(t) = \begin{cases} 0, & t < 0 \\ u_*, & t > 0 \end{cases}; \quad a(t) = \begin{cases} a_0, & t < 0 \\ a_0 e^{\beta \omega_0 t}, & t > 0 \end{cases} \quad (1.1a,b)$$

and

(ii) the spatial growth scenario

$$U^*(x) = \begin{cases} 0, & x < 0 \\ u_*, & x > 0 \end{cases}; \quad a(x) = \begin{cases} a_0, & x < 0 \\ a_0 e^{\alpha k_0 x}, & x > 0 \end{cases}. \quad (1.2a,b)$$

In (1.1b) and (1.2b), β and α are the temporal and spatial growth rates, respectively, and to lowest order, $\beta = \alpha/2$ (Gaster 1962). For the sake of completeness, it is worthwhile to mention that other scenarios of combined growth are, of course, possible. Generally speaking, α and β depend on the shear velocity and on the wavenumber k_0 [or wave frequency $\omega_0 = (gk_0)^{1/2}$]. However, the actual rate of energy transfer from the wind to the waves depends also on a_0 itself. In linear stability studies, one is interested, among others, to detect the fastest growing mode (wavenumber). Here it is suggested to widen this interest and to look also at the fastest energy-accumulating modes under several scenarios. The aim of this paper is twofold:

- (i) to investigate the accuracy of the relation $\beta = \alpha/2$ and
- (ii) to find which wave modes (i.e., which parts of the spectrum) are absorbing most of the energy from the wind, in both of the aforementioned scenarios and for young/mature sea states.

In this paper we restrict the discussion to gravity waves and assume a steady shear velocity in the air. The

¹ In this study it is assumed that the wind profile is completely defined by the shear velocity.

Corresponding author address: M. Stiassnie, Faculty of Civil and Environmental Engineering, Technion—Israel Institute of Technology, Haifa 32000, Israel.
E-mail: miky@tx.technion.ac.il

only effect of turbulence that enters our derivation is its effect on the mean wind profile.

The mathematical problem is formulated in section 2, and three different methods of solution are discussed in section 3. The issues of comparison between temporal and spatial growth and of the fastest-growing modes (for young and mature seas) are treated in sections 4 and 5, respectively. Conclusions are drawn in section 6.

2. Mathematical formulation

Assuming two-dimensional inviscid and incompressible flows in the water (denoted by subscript w), as well as in the air (denoted by subscript a) above it, and relatively small wavy components superposed on steady, leading order given, shear flows, the velocities, pressures, and densities are denoted by

- horizontal air velocity component: $U_a(z) + u_a(x, z, t)$;
- vertical air velocity component: $v_a(x, z, t)$;
- air pressure: $P_0 - g\rho_a z + p_a(x, z, t)$, where ρ_a is the density of the air;
- horizontal water velocity component: $U_w(z) + u_w(x, z, t)$;
- vertical water velocity component: $v_w(x, z, t)$;
- water pressure: $P_0 - g\rho_w z + p_w(x, z, t)$, where ρ_w is the density of water, and P_0 is a constant reference pressure: U_a and U_w are the prescribed unperturbed wind and current, respectively.

Note that lowercase letters indicate fluctuating quantities.

The wavy interface between the water and the air is $z = \eta(x, t)$. The continuity equations and the linearized equations of motion are

$$\frac{\partial u_w}{\partial x} + \frac{\partial v_w}{\partial z} = 0, \quad z \leq 0, \quad (2.1a)$$

$$\frac{\partial u_w}{\partial t} + U_w \frac{\partial u_w}{\partial x} + U'_w v_w = -\frac{1}{\rho_w} \frac{\partial p_w}{\partial x}, \quad z \leq 0, \quad (2.1b)$$

$$\frac{\partial v_w}{\partial t} + U_w \frac{\partial v_w}{\partial x} = -\frac{1}{\rho_w} \frac{\partial p_w}{\partial z}, \quad z \leq 0, \quad (2.1c)$$

$$\frac{\partial u_a}{\partial x} + \frac{\partial v_a}{\partial z} = 0, \quad z \geq 0, \quad (2.2a)$$

$$\frac{\partial u_a}{\partial t} + U_a \frac{\partial u_a}{\partial x} + U'_a v_a = -\frac{1}{\rho_a} \frac{\partial p_a}{\partial x}, \quad z \geq 0, \quad (2.2b)$$

and

$$\frac{\partial v_a}{\partial t} + U_a \frac{\partial v_a}{\partial x} = -\frac{1}{\rho_a} \frac{\partial p_a}{\partial z}, \quad z \geq 0. \quad (2.2c)$$

In the above equations, the prime denotes differentiation with respect to the vertical coordinate, z .

The systems (2.1) and (2.2) have wavy solutions with wavenumber k and frequency ω :

$$u_w = a_0 f'_w e^{i(kx - \omega t)}, \quad v_w = -ika_0 f_w e^{i(kx - \omega t)}, \quad (2.3a,b)$$

$$p_w = a_0 \frac{\rho_w}{k} [(\omega - kU_w) f'_w + kU'_w f_w] e^{i(kx - \omega t)}, \quad (2.3c)$$

$$u_a = a_0 f'_a e^{i(kx - \omega t)}, \quad v_a = -ika_0 f_a e^{i(kx - \omega t)}, \quad \text{and} \quad (2.4a,b)$$

$$p_a = a_0 \frac{\rho_a}{k} [(\omega - kU_a) f'_a + kU'_a f_a] e^{i(kx - \omega t)}, \quad (2.4c)$$

where the auxiliary functions f_w and f_a satisfy Rayleigh's equation

$$f''_w - \left(k^2 + \frac{U''_w}{U_w - \omega/k} \right) f_w = 0, \quad z \leq 0 \quad (2.5)$$

and

$$f''_a - \left(k^2 + \frac{U''_a}{U_a - \omega/k} \right) f_a = 0, \quad z \geq 0. \quad (2.6)$$

Note that the real part of a complex quantity represents the physical variable.

For the interface with initial amplitude a_0 ,

$$\eta = a_0 e^{i(kx - \omega t)}, \quad (2.7)$$

the linearized kinematic and dynamic free-surface boundary conditions are

$$v_w = \frac{\partial \eta}{\partial t} + U_w \frac{\partial \eta}{\partial x}; \quad v_a = \frac{\partial \eta}{\partial t} + U_a \frac{\partial \eta}{\partial x}, \quad z = 0, \quad (2.8a,b)$$

and

$$p_w - g\rho_w \eta = p_a - g\rho_a \eta - \rho_w \tau \frac{\partial^2 \eta}{\partial x^2}, \quad z = 0, \quad (2.9)$$

where τ is the surface tension divided by the density of the water.

In terms of the auxiliary functions, (2.8) and (2.9) reduce to

$$f_w(0) = \frac{\omega}{k} - U_w(0), \quad f_a(0) = \frac{\omega}{k} - U_a(0), \quad (2.10a,b)$$

and

$$(\omega - kU_w)(f'_w + U'_w) - gk - \tau k^3 = \rho[(\omega - kU_a) \times (f'_a + U'_a) - gk] \quad \text{at } z = 0, \quad (2.11)$$

where $\rho = \rho_a/\rho_w$.

Equation (2.11) is a dispersion equation, giving the relation between the frequency ω and wavenumber k .

Restricting the discussion to shear flows for which $U_a''(\infty)$ and $U_w''(-\infty)$ tend to zero, the two additional boundary conditions for the auxiliary functions are

$$f_w'' - kf_w' = 0, z \rightarrow -\infty \quad \text{and} \quad (2.12a)$$

$$f_a'' + kf_a' = 0, z \rightarrow \infty. \quad (2.12b)$$

For cases with a negligible current in the water, the solution of (2.5), (2.10a), and (2.12a) is

$$f_w = \frac{\omega}{k} e^{kz}. \quad (2.13)$$

Substituting (2.13) into (2.11) and neglecting the influence of surface tension gives

$$\omega^2 - gk = \rho[(\omega - kU_a)(f_a' + U_a') - gk] \quad \text{at} \quad z = 0. \quad (2.14)$$

The numerical examples in this paper are restricted to logarithmic wind profiles

$$U_a = \frac{u_*}{\kappa} \ln\left(1 + \frac{z}{z_0}\right), \quad z \geq 0, \quad (2.15)$$

where $\kappa = 0.41$ is von Kármán's constant, u_* is the so-called shear velocity, and the roughness z_0 is given by Charnock's relation with constant α_{Ch} :

$$z_0 = \alpha_{\text{Ch}} u_*^2 / g. \quad (2.16)$$

The methods of solution are outlined in the following section.

3. Methods of solution

To find f_a , for given k and ω , one has to solve

$$f_a'' - \left(k^2 + \frac{U_a''}{U_a - \omega/k}\right) f_a = 0, \quad z \geq 0 \quad (3.1)$$

with the two boundary conditions

$$f_a(0) = \omega/k, f_a'(\infty) = -kf_a'(\infty); \quad (3.2a,b)$$

see (2.6), (2.10b), (2.15), and (2.12b).

However, one cannot choose k and ω freely since they have to fulfill the dispersion relation

$$\omega^2 - gk = \rho\{\omega[f_a'(0) + u_*/\kappa z_0] - gk\}; \quad (3.3)$$

see (2.14) and (2.15).

Owing to the influence of the wind, the frequency ω and the wavenumber k can have small but important deviations from their values ω_0 and k_0 in windless conditions. This fact is made explicit by the notation

$$\omega = \omega_0 + \omega_1; |\omega_1|/\omega_0 \ll 1 \quad \text{and} \quad (3.4a)$$

$$k = k_0 + k_1; |k_1|/k_0 \ll 1, \quad (3.4b)$$

where ω_1 and k_1 can be complex and

$$\omega_0^2 = gk_0, \quad (3.5)$$

is the windless dispersion relation.

At least three methods of solution are possible; they will be referred to as the singular approach, exact approach, and higher-order solution for spatiotemporal growth—for reasons to become obvious later.

a. The singular approach

In this approach (ω, k) are replaced by ω_0 and k_0 in (3.1), (3.2a,b) as well as on the rhs of (3.3) and by (3.4a,b) on the lhs of (3.3):

$$f_a'' - \left(k_0^2 + \frac{U_a''}{U_a - \omega_0/k_0}\right) f_a = 0, \quad z \geq 0, \quad (3.6)$$

$$f_a(0) = \omega_0/k_0, f_a'(\infty) = -k_0 f_a'(\infty), \quad \text{and} \quad (3.7a,b)$$

$$\omega_1^2 + 2\omega_0\omega_1 - gk_1 = \rho\omega_0[f_a'(0) + u_*/\kappa z_0 - \omega_0]. \quad (3.8)$$

Neglecting the small first term on the lhs of (3.8) and then dividing by $2\omega_0$ gives

$$\omega_1 - c_{g_0} k_1 = \frac{\rho}{2}[f_a'(0) + u_*/\kappa z_0 - \omega_0], \quad (3.9)$$

where $c_{g_0} = g/2\omega_0$ is the group velocity.

Equation (3.6) is singular at the so-called critical layer, where $U_a = c_0$, $c_0 = \omega_0/k_0$, is the phase velocity. This singular equation has been solved by Conte and Miles (1959), Janssen (1991), and Beji and Nadaoka (2004), among others.

Taking the imaginary part of (3.9) and recognizing that

$$\text{Im}\{\omega_1\} = \frac{\partial a / \partial t}{a}; \quad \text{Im}\{k_1\} = -\frac{\partial a / \partial x}{a}$$

are the temporal and spatial growth rates of the amplitude a (i.e., one-half of the wave height, $a > 0$), respectively, one obtains

$$\frac{\partial a}{\partial t} + c_{g_0} \frac{\partial a}{\partial x} = \frac{\rho a}{2} \text{Im}\{f_a'(0)\}. \quad (3.10)$$

Equation (3.10) is rewritten in terms of energy as

$$\frac{\partial(a^2)}{\partial t} + c_{g_0} \frac{\partial(a^2)}{\partial x} = \rho a^2 \text{Im}\{f_a'(0)\}. \quad (3.11)$$

Note that the first/second term on the lhs of (3.11) vanishes for pure spatial/temporal growth conditions. In any case, it turns out that ω_1 or k_1 (or both) have imaginary parts so that the original Rayleigh equation (3.1) is actually *regular*, which leads us to the following two additional methods of solution.

b. The exact approach

Substituting (3.4a,b) into (3.1), (3.2a,b) and (3.3) yields

$$f_a'' - \left[(k_0 + k_1)^2 + \frac{U_a''}{U_a - c_0/(1 + k_1/k_0)} \right] f_a = 0, \quad z \geq 0, \tag{3.12}$$

$$f_a(0) = (\omega_0 + \omega_1)/(k_0 + k_1); \quad f_a'(\infty) = -(k_0 + k_1)f_a(\infty), \tag{3.13a,b}$$

and

$$(\omega_0 + \omega_1)^2 - g(k_0 + k_1) = \rho \{ (\omega_0 + \omega_1) [f_a'(0) + u_*/\kappa z_0] - g(k_0 + k_1) \}. \tag{3.14}$$

In the above system, U_a , k_0 , and $\omega_0 = \sqrt{gk_0}$ are given and $f_a(z)$, k_1 , and ω_1 are unknowns to be found simultaneously. It is quite clear that the system (3.12)–(3.14) has too many unknowns, and either k_1 or ω_1 has to be omitted, that is, set to zero. Note that the case $k_1 \equiv 0$ corresponds to pure temporal growth, whereas $\omega_1 \equiv 0$ corresponds to pure spatial growth. It is self-evident that for these two special cases the above regular equation is the exact equation for the problem at hand, whereas the singular approach should be treated as its approximation.

1) TEMPORAL GROWTH

Substituting $k_1 = 0$ in (3.12), (3.13a,b), and (3.14) gives

$$f_a'' - \left\{ k_0^2 + \frac{U_a''}{U_a - c_0(1 + \omega_1/\omega_0)} \right\} f_a = 0, \quad z \geq 0 \tag{3.15}$$

$$f_a(0) = c_0 \left(1 + \frac{\omega_1}{\omega_0} \right), \quad f_a'(\infty) = -k_0 f_a(\infty) \tag{3.16a,b}$$

$$2\omega_0\omega_1 + \omega_1^2 = \rho \{ (\omega_0 + \omega_1) (f_a'(0) + u_*/\kappa z_0) - \omega_0^2 \} \tag{3.17}$$

2) SPATIAL GROWTH

Substituting $\omega_1 = 0$ in (3.12), (3.13a,b), and (3.14),

$$f_a'' - \left[(k_0 + k_1)^2 + \frac{U_a''}{U_a - c_0/(1 + k_1/k_0)} \right] f_a = 0, \quad z \geq 0, \tag{3.18}$$

$$f_a(0) = c_0 \left/ \left(1 + \frac{k_1}{k_0} \right) \right.; \quad f_a'(\infty) = -(k_0 + k_1)f_a(\infty), \tag{3.19a,b}$$

and

$$-gk_1 = \rho \{ \omega_0 [f_a'(0) + u_*/\kappa z_0] - g(k_0 + k_1) \}. \tag{3.20}$$

The method of solution of the exact approach is the same for the spatial and temporal cases and is outlined for the latter. Equation (3.15) is of second order but has to obey three boundary conditions: (3.16a,b) and (3.17). The first two are used while solving the Rayleigh equation (3.15) for a given value of ω_1 , whereas the dynamic boundary condition (3.17) is used to obtain the following iteration for ω_1 , until a specified number of significant digits remains unchanged. The iteration is started with a “first guess” imaginary value for ω_1 .

In solving the ODE (3.15), a large value of z is chosen, typically $k_0 z_\infty = 100$, where (3.16b) is replaced by

$$f_a = 1; \quad f_a' = -k_0 \quad \text{at} \quad z = z_\infty. \tag{3.21}$$

Equation (3.15) is solved by stepping from z_∞ to $z = 0$, using Mathematica’s solver, and then normalizing to satisfy the kinematic boundary condition (3.16a). Table 1 demonstrates the convergence of the process, for the example with $\alpha_{Ch} = 0.0178$, $u_* = 0.08c_0$, and $\rho = 10^{-3}$.

Note that the deviation of the new (exact approach) results from singular (critical layer) calculations, for the temporal scenario, is less than 10%; see appendix. A similar iterative method was used by Morland et al. (1991) to study another instability problem. The limitation of the exact solution is its inability to treat the combined growth problem, a difficulty which is overcome by the third method of solution.

c. Higher-order solution for spatiotemporal growth

Taking the expansion of f_a to first order in ω_1 and k_1 :

$$f_a = f_0 + f_\omega \omega_1 + f_k k_1 + O(\omega_1^2, k_1^2, \omega_1 k_1). \tag{3.22}$$

Equations (3.12)–(3.14) can now be expanded in orders of ω_1 and k_1 . The leading order gives (3.6)–(3.8). At the next order we have a system for f_ω :

TABLE 1. Demonstration of convergence for two values of $k_0 z_\infty$: $u_*/c = 0.08$, $\rho = 0.001$, $\kappa = 0.41$, and $\alpha_{\text{ch}} = 0.0178$.

Iteration	ω/ω_0 for $k_0 z_\infty = 100$	ω/ω_0 for $k_0 z_\infty = 10$
1	1.0 + 0.0001 <i>i</i>	1.0 + 0.0001 <i>i</i>
2	0.999 651 + 0.000 081 505 8 <i>i</i>	0.999 651 + 0.000 081 505 8 <i>i</i>
3	0.999 493 + 0.000 073 111 3 <i>i</i>	0.999 493 + 0.000 073 111 3 <i>i</i>
4	0.999 420 + 0.000 069 299 5 <i>i</i>	0.999 420 + 0.000 069 299 4 <i>i</i>
5	0.999 387 + 0.000 067 568 3 <i>i</i>	0.999 387 + 0.000 067 568 2 <i>i</i>
6	0.999 372 + 0.000 066 781 9 <i>i</i>	0.999 372 + 0.000 066 781 9 <i>i</i>
7	0.999 366 + 0.000 066 424 7 <i>i</i>	0.999 366 + 0.000 066 424 7 <i>i</i>
8	0.999 362 + 0.000 066 262 5 <i>i</i>	0.999 362 + 0.000 066 262 5 <i>i</i>
9	0.999 361 + 0.000 066 188 8 <i>i</i>	0.999 361 + 0.000 066 188 8 <i>i</i>
10	0.999 360 + 0.000 066 155 3 <i>i</i>	0.999 360 + 0.000 066 155 3 <i>i</i>
11	0.999 360 + 0.000 066 140 1 <i>i</i>	0.999 360 + 0.000 066 140 1 <i>i</i>
12	0.999 360 + 0.000 066 133 2 <i>i</i>	0.999 360 + 0.000 066 133 2 <i>i</i>
13	0.999 360 + 0.000 066 130 1 <i>i</i>	0.999 360 + 0.000 066 130 1 <i>i</i>
14	0.999 360 + 0.000 066 128 7 <i>i</i>	0.999 360 + 0.000 066 128 6 <i>i</i>
15	0.999 360 + 0.000 066 128 0 <i>i</i>	0.999 360 + 0.000 066 128 0 <i>i</i>
16	0.999 360 + 0.000 066 127 7 <i>i</i>	0.999 360 + 0.000 066 127 7 <i>i</i>
17	0.999 360 + 0.000 066 127 6 <i>i</i>	0.999 360 + 0.000 066 127 6 <i>i</i>
18	0.999 360 + 0.000 066 127 5 <i>i</i>	0.999 360 + 0.000 066 127 5 <i>i</i>
19	0.999 360 + 0.000 066 127 5 <i>i</i>	0.999 360 + 0.000 066 127 5 <i>i</i>
20	0.999 360 + 0.000 066 127 5 <i>i</i>	0.999 360 + 0.000 066 127 5 <i>i</i>
21	0.999 360 + 0.000 066 127 5 <i>i</i>	0.999 360 + 0.000 066 127 4 <i>i</i>
22	0.999 360 + 0.000 066 127 5 <i>i</i>	0.999 360 + 0.000 066 127 4 <i>i</i>
23	0.999 360 + 0.000 066 127 5 <i>i</i>	0.999 360 + 0.000 066 127 4 <i>i</i>

$$f''_\omega - \left(k_0^2 + \frac{U_a''}{U_a - \omega_0/k_0} \right) f_\omega = \gamma f_0, \quad z \geq 0, \quad (3.23)$$

$$\gamma = U_a''/k_0/(U_a - \omega_0/k_0)^2, \quad (3.24)$$

and

$$f_\omega(0) = 1/k_0; \quad f'_\omega(\infty) = -k_0 f_\omega(\infty) \quad (3.25a,b)$$

and a system for f_k :

$$f''_k - \left(k_0^2 + \frac{U_a''}{U_a - \omega_0/k_0} \right) f_k = \frac{-\omega_0}{k_0} \gamma f_0 + 2k_0 f_0; \quad (3.26)$$

$$f_k(0) = \frac{-\omega_0}{k_0^2}; \quad f'_k(\infty) = -f_0(\infty) - k_0 f_k(\infty). \quad (3.27a,b)$$

Expanding (3.14) to $O(\omega_1, k_1)$ leads to

$$\omega_1 - (c_{g_0} + c_{g_1})k_1 = \frac{\rho}{2} \left[f'_0(0) + \frac{u_*}{\kappa z_0} - \omega_0 \right] / \left\{ 1 - \frac{\rho}{2} \left[\frac{f'_0(0)}{\omega_0} + \frac{u_*}{\kappa z_0 \omega_0} + f'_\omega(0) \right] \right\}, \quad (3.28a)$$

where

$$c_{g_1} = \frac{\rho}{2} \left[\frac{\omega_0}{g} f'_k(0) - 1 + \frac{f'_0(0)}{\omega_0} + \frac{u_*}{\kappa z_0 \omega_0} + f'_\omega(0) \right] c_{g_0}. \quad (3.28b)$$

The imaginary part of (3.28a) reduces to (3.9) at leading order and leads to an evolution equation corresponding to (3.11). The values of $f'_0(0)$, $f'_\omega(0)$, and $f'_k(0)$ can be found without solving the singular Eqs. (3.6), (3.23), and (3.26). Instead, we solve (3.12) and (3.13) with three sets of values for (ω_1, k_1) (choosing complex values, to avoid singularity). If the values for (ω_1, k_1) are small enough, we can extract the above three values of $f'_0(0)$, $f'_\omega(0)$, and $f'_k(0)$ from the three values of $f'_a(0)$ and Eq. (3.22). The computational results for temporal/spatial growth scenarios agree with the results of the exact method.

4. Comparison between spatial and temporal growth conditions

For temporal or spatial growth, respectively: k or ω is kept constant that is, ($k = k_0$ or $\omega = \omega_0$), $\text{Im}\{\omega\}$ or $\text{Im}\{-k\}$ provide the growth rates, and $\text{Re}\{\omega\}$ (or $\text{Re}\{k\}$) are slightly different from ω_0 (or k_0). These slight changes as functions of u_*/c_0 hardly exceed 6%, as one can see from Fig. 1.

The ratio of the dimensionless spatial growth rate α to its temporal counterpart β is given in Fig. 2:

$$\alpha = -\text{Im}\{k\}/k_0; \quad \beta = \text{Im}\{\omega\}/\omega_0. \quad (4.1)$$

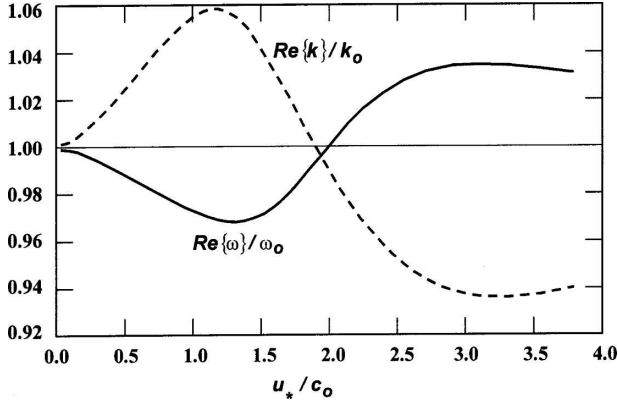


FIG. 1. Variation of frequency $\text{Re}\{\omega\}$ for temporal growth (solid line) and variation of wavenumber $\text{Re}\{k\}$ for spatial growth (dashed line) for $\alpha_{\text{Ch}} = 0.0144$ and $\rho = 0.00125$.

Note that the ratio α/β varies in the range 1.75 to 2.4, which is within 20% of the value 2 (the ratio of the phase velocity to the group velocity), predicted by (3.9) and by Gaster (1962). Note that (3.9) also predicts

$$(\text{Re}\{k_1\}/k_0)/(\text{Re}\{\omega_1\}/\omega_0) = -2, \quad (4.2)$$

as is clearly reflected in Fig. 1.

5. On the fastest energy-accumulating modes

Figure 3 gives the newly calculated temporal growth rate for $\alpha_{\text{Ch}} = 0.0144$ and $\rho = 1/800$, together with previously published results from Komen et al. (1994). The main difference between the new result and that of Komen et al. is in the maximum found near $u_*/c_0 = 2$, which identifies a fastest-growing mode (i.e., largest β) for a given shear velocity u_* . Note that the experimental data for large u_*/c_0 is already within the gravity-capillary range, whereas both theoretical lines are for pure gravity waves.

The related, fastest energy-accumulating modes, for

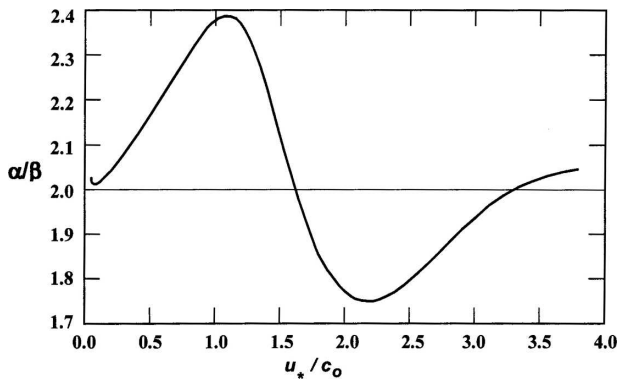


FIG. 2. Ratio of spatial to temporal growth rates, for $\alpha_{\text{Ch}} = 0.0144$, $\rho = 1/800$.

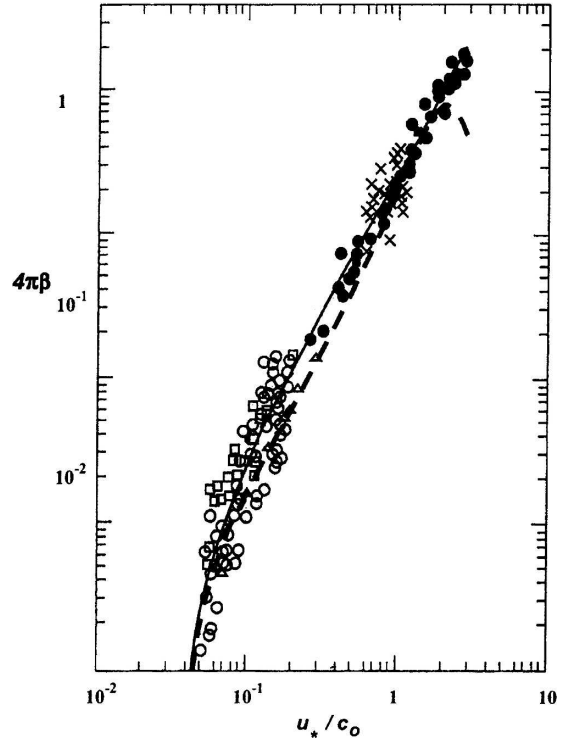


FIG. 3. Temporal growth rate (solid line) from Komen et al. (1994, p. 85); new calculation with $\alpha_{\text{Ch}} = 0.0144$ and $\rho = 1/800$ (dashed line). Different symbols represent experimental results from various authors; for details see Fig. 2 of Plant (1982).

four different physical scenarios are addressed next. These scenarios are as follows: (I) temporal growth where all modes have the same initial amplitude a_0 ; (II) temporal growth where all modes have the same initial steepness $\epsilon_0 = ak$; (III) and (IV) similar to (I) and (II), respectively, but for spatial growth conditions. To achieve the above goal one has to nondimensionalize the dependent variables $d(a^2)/dt$ and $d(a^2)/dx$ by using $(a_0, g, \text{ and } u_*)$ for cases I and III and by using $(\epsilon_0, g, \text{ and } u_*)$ for cases II and IV. From dimensional considerations one can show that

$$\frac{u_*}{ga_0^2} \frac{d(a^2)}{dt} = 2(u_*/c)\beta; \quad \frac{g}{\epsilon_0^2 u_*^3} \frac{d(a^2)}{dt} = 2(c/u_*)^3 \beta \quad (5.1a,b)$$

and

$$\frac{u_*^2}{ga_0^2} \frac{d(a^2)}{dx} = 2(u_*/c)^2 \alpha; \quad \frac{g}{\epsilon_0^2 u_*^2} \frac{d(a^2)}{dx} = 2(c/u_*)^2 \alpha. \quad (5.1c,d)$$

Note that different length scales have been used to normalize a and x in (5.1c,d), which is appropriate because of the linear nature of the problem.

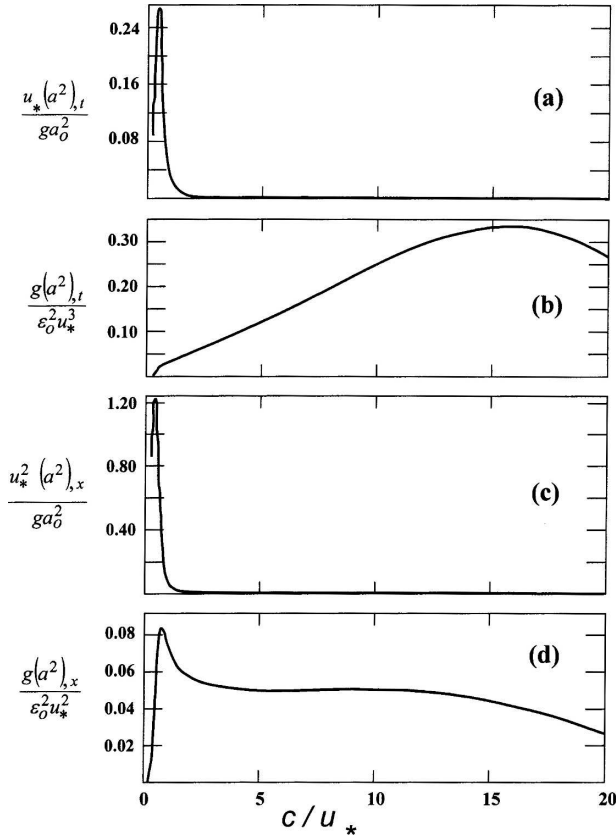


FIG. 4. Modal distribution of energy input from wind to waves: (a) Temporal growth, all modes start with the same amplitude a_0 ; (b) temporal growth, all modes start with the same steepness ε_0 ; (c), (d) similar to (a), (b) but for spatial growth.

The results are depicted in Fig. 4 as functions of the independent variable c/u_* ; the maxima and the ranges of c/u_* for which the energy-accumulating range is larger than half of the appropriate maximum are given in Table 2.

For young seas, where all modes are assumed to have the same initial amplitude (see cases I and III), most of the energy goes into the very short waves, $c/u_* \in (0.1, 0.7)$ and no substantial difference between the temporal and spatial scenarios is detected. For mature seas, where all modes are assumed to have the same initial steepness ε_0 , a profound difference between the two scenarios occurs. For the temporal cases, most of the energy goes into rather long waves $c/u_* > 7$; whereas, for its spatial parallel, the energy goes into a wide range of modes $c/u_* \in (0.5, 17)$.

6. Summary

The study of the growth of waves under the influence of wind using the Miles theory, which was started al-

TABLE 2. Fastest energy-accumulation modes.

Case	Location of maximum c/u_*	Range of substantial energy accumulation
I	0.44	0.3–0.7
II	16	7–20
III	0.35	0.1–0.6
IV	0.74	0.5–17

most 50 years ago (Miles 1957), is continuing to stimulate the interest of the scientific community. Such studies find their main application in improving the accuracy of wave-forecasting models.

The present paper addressed a few issues, some of which help to obtain new answers, and others open

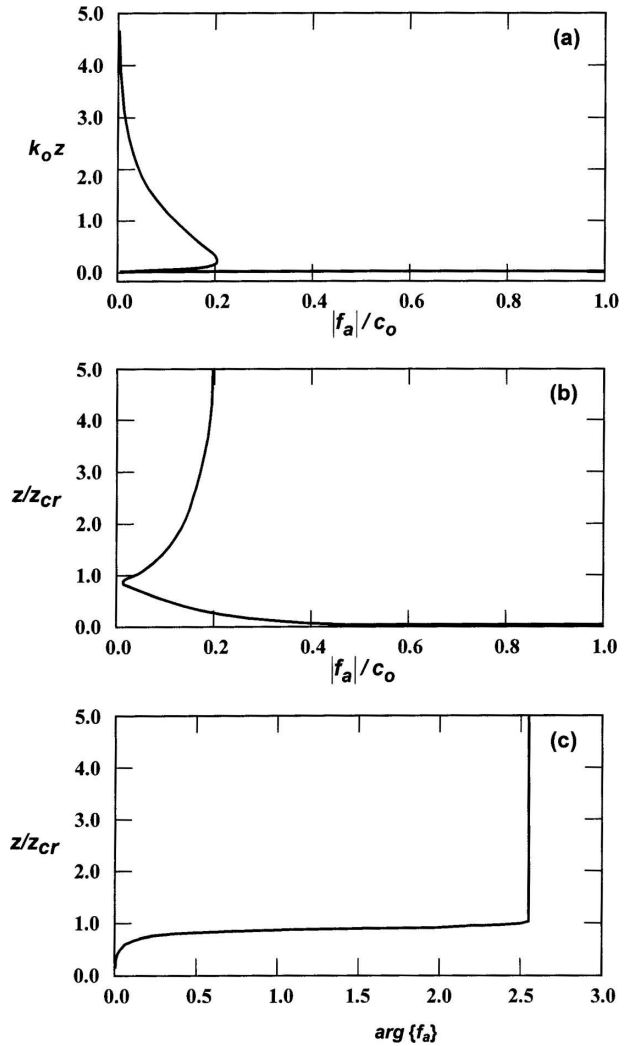


FIG. 5. The auxiliary function $f_a(z)$, for $\alpha_{ch} = 0.0178$, $\rho = 10^{-3}$, and $u_* = 0.067c_0$. (a), (b) The modulus of the complex function f_a , and (c) its argument.

TABLE A1. Normalized growth rate $2\omega_0\text{Im}\{\omega_1\}/\rho k_0^2 U_1^2$ from three different sources.

c_0/U_1	u_{*c}/c_0	New calculation (exact approach)	Conte and Miles (1959) (singular approach)	Beji and Nadaoka (2004) (singular approach)
1	0.4	3.57	3.54	3.53
2	0.2	3.43	3.41	3.41
3	0.13	3.44	3.43	3.43
4	0.1	3.44	3.43	3.43
5	0.08	3.31	3.30	3.30
6	0.067	2.98	2.98	2.97
7	0.057	2.45	2.44	2.44
8	0.05	1.76	1.75	1.75
9	0.044	1.02	1.02	1.02
10	0.4	0.410	0.405	0.405
11	0.036	0.0742	0.0725	—
12	0.033	0.001 88	0.001 77	—

further questions. These issues are mentioned below in order of appearance:

- (i) A method of solution, called the exact approach, that circumvents the critical-layer singularity was adopted. The deviations between this method and the standard singular approach were found to be less than 10%.
- (ii) The spatial growth rate was computed directly. The ratio of the spatial to temporal growth rates was shown to deviate by up to 20% from the leading-order value of c/c_g .
- (iii) An efficient higher-order solution method was introduced that closely reproduced the exact approach results.
- (iv) The wave modes that extract most of the energy from the wind were found, as one would expect, to depend on the actual sea condition. The profound difference in the range of substantial energy input, between temporal growth and spatial growth for a “mature” sea, seems less intuitive.

Note that the maximum growth rate in Fig. 3 and the maxima in Figs. 4a, 4c, and 4d are for a small c/u_* value. Unless u_* , and also $U_{10} = U_a|_{z=10\text{m}}$, are very large (U_{10} beyond 20 m s^{-1}), these waves are within the gravity–capillary range. A more detailed study of these maxima for less strong winds will require including the surface tension term.

Last, the auxiliary function $f_a(z)$ is illustrated in Fig. 5, which demonstrates how different it is from $\exp(-k_0z)$. The large derivatives for $z \leq z_{\text{cr}}$ indicate the possible importance of viscous terms. Nevertheless, for large enough z , the relative deviation of $|f_a(z)|$ from an exponential decay, that is, the quantity $|\text{const}|f_a| - e^{-k_0z}|/e^{-k_0z}$, is less than 1% for $z > (2\pi/k_0)$ and less than 1‰ for $z > 10(2\pi/k_0)$.

Acknowledgments. This research was supported by the Israel Science Foundation (Grant 695/04) and by the Fund for Promotion of Research at the Technion.

APPENDIX

Comparison between the Exact and Singular Approaches

The exact method of solution is essentially different from the singular critical layer approach and is expected to provide improved results. In Table A1, new results by the exact approach for the normalized temporal growth rate are compared with those of Conte and Miles (1959), and Beji and Nadaoka (2004), using their normalization, their coefficients $\alpha_{\text{Ch}} = 0.0178$, $\rho = 10^{-3}$, and their values of c_0/U_1 , where $U_1 = u_{*c}/\kappa$.

The deviation of the new (exact approach) results from previous (critical layer) calculations is less than 7%. Conte and Miles, as well as Beji and Nadaoka, do not provide results for values of u_{*c}/c_0 larger than 0.4. In this range of larger values of u_{*c}/c_0 , the method used by Janssen (1991) gives accurate results.

Rerunning the critical layer subroutine, written by Janssen (1991), for $\rho = 0.001 225$ and $\alpha_{\text{Ch}} = 0.0144$, we have obtained the comparison presented in Table A2.

TABLE A2. Normalized growth rate $4\pi\text{Im}\{\omega_1\}/\omega_0$ from two sources.

u_{*c}/c_0	New calculation exact approach	Janssen (1991) singular approach
0.1	0.0017	0.0016
0.2	0.0066	0.0064
0.3	0.015	0.015
0.5	0.045	0.043
1	0.22	0.20
1.5	0.59	0.54
3	0.45	0.43

The new results are within 10% of those obtained by the critical layer method.

REFERENCES

- Beji, S., and K. Nadaoka, 2004: Solution of Rayleigh's instability equation for arbitrary wind profiles. *J. Fluid Mech.*, **500**, 65–73.
- Conte, S. D., and J. W. Miles, 1959: On the integration of Orr–Sommerfeld equation. *J. Soc. Indust. Appl. Maths*, **7**, 361–369.
- Gaster, M., 1962: A note on the relation between temporally-increasing and spatially-increasing disturbances in hydrodynamic stability. *J. Fluid Mech.*, **14**, 222–224.
- Janssen, P. A. E. M., 1991: Quasi-linear theory of wind wave generation applied to wave forecasting. *J. Phys. Oceanogr.*, **21**, 1631–1642.
- Komen, G. J., L. Cavaleri, M. Donelan, K. Hasselmann, S. Hasselmann, and P. A. E. M. Janssen, 1994: *Dynamics and Modelling of Ocean Waves*. Cambridge University Press, 532 pp.
- Miles, J. W., 1957: On the generation of surface waves by shear flows. *J. Fluid Mech.*, **3**, 185–204.
- Morland, L. C., P. G. Saffman, and H. C. Yuen, 1991: Waves generated by shear layer instabilities. *Proc. Roy. Soc. London*, **A433**, 441–450.
- Plant, W. J., 1982: A relationship between wind stress and wave slope. *J. Geophys. Res.*, **87** (C3), 1961–1967.
- Rayleigh, L., 1880: On the stability or instability of certain fluid motions. *Proc. London Math. Soc.*, **11**, 57–70.